Direct pickup and knockout processes in inclusive (p, αx) reactions from 42 to 300 MeV

Uozumi, Yusuke
Department of Applied Quantum Physics and Nuclear Engineering, Kyushu University

Fukuda, Yuki
Department of Applied Quantum Physics and Nuclear Engineering, Kyushu University

山口, 雄司
Department of Applied Quantum Physics and Nuclear Engineering, Kyushu University

Watanabe, Gaku
Department of Applied Quantum Physics and Nuclear Engineering, Kyushu University

他

出版情報：PHYSICAL REVIEW C. 102, pp.014604-, 2020-07-09. American Physical Society
バージョン：

Direct pickup and knockout processes in inclusive $(p, \alpha x)$ reactions from 42 to 300 MeV

Yusuke Uozumi,[1] Yuki Fukuda,[1] Yuji Yamaguchi,[1] Gaku Watanabe,[1] and Masahiro Nakano[1,2]
[1]*Department of Applied Quantum Physics and Nuclear Engineering, Kyushu University, 744 Motooka, Nishi-ku, Fukuoka 819-0395, Japan*
[2]*Junshin Gakuen University, 1-1-1 Chikushigaoka, Minami-ku, Fukuoka 815-8510, Japan*

(Received 8 March 2020; accepted 15 June 2020; published 9 July 2020)

Inclusive $(p, \alpha x)$ reactions from 42 to 300 MeV are investigated to quantitatively understand the roles of direct pickup and knockout processes. These two processes as well as indirect pickup are incorporated into the intranuclear cascade model. Calculations followed by the evaporation model successfully explain the double-differential cross-section spectra in terms of both shape and magnitude. Direct pickup occupies the low excitation energies of the spectra, and knockout appears between the direct pickup and evaporation regions. The contribution of knockout is negligible below 100 MeV, increases to be comparable with that of direct pickup at 160 MeV, and is dominant above 200 MeV. Indirect pickup shows an important contribution at 300 MeV. The direct pickup and knockout processes show decreasing trends of incident-energy dependence, common to targets ranging from ^{12}C to ^{209}Bi. However, the decrease of direct pickup is much faster than that for knockout.

DOI: 10.1103/PhysRevC.102.014604

I. INTRODUCTION

The mechanism of α production in proton-nucleus reactions involves direct pickup, knockout (including knockon), and indirect pickup processes, excluding the evaporation process. The contributions of the direct pickup and knockout processes have been an important issue [1] in elucidating the mechanism of exclusive (p, α) reactions to discrete states. At energies of 50 MeV or less, the angular distributions of some transitions have been analyzed in terms of the differential cross section $d\sigma/d\Omega$ and analyzing power A_y by using distorted-wave Born approximation (DWBA) theory. Bonetti *et al.* [2] concluded that transitions to levels near the ground state are due to direct pickup and those to excited states around 5 MeV are due to knockout. Meanwhile, Gadioli *et al.* [3] pointed out serious ambiguities in DWBA calculations, which are sensitive to optical-model potential parameters and various assumptions involved in the form factor in particular, because the differing formalism between the pickup and knockon (knockout) calculations is aggregated to the proton exchange. As a result, they demonstrated that the knockout calculation can reproduce the experimental data to the same extent as the pickup calculation, even for the ground-state transition.

More recently [4], preequilibrium model analyses have been conducted within the Feshbach-Kerman-Koonin (FKK) formulation [5,6] for ^{93}Nb(p, α) reactions at incident energies of 65–160 MeV. Although the angular distributions of $d\sigma/d\Omega$ and A_y were successfully reproduced, the model required a reaction mechanism with an unnatural incident-energy trend: Knockout governed the reaction at 65 and 160 MeV, but pickup played a major role at the intermediate energy of 100 MeV. Subsequently, Cowley *et al.* [7] proposed an explanation for this strange energy dependence and pointed out the importance of information about the kinematics. Note, however, that an open problem [8] remains in the justification of the FKK formalism. In addition, a common shortcoming of FKK and DWBA is that the kinematics of two-body collision is not explicitly considered, even though the kinematics is the essential difference between pickup and knockout. The knockout strength is suppressed because of the discrete-level constraint [9,10] when the scattered proton is found in either a virtual state or a lower energy state. Therefore, the transition to the ground state via knockout must be imperceptible. It is also anticipated that the contribution of knockout becomes greater with increasing incident energy, because more phase space is allowed for the scattered proton.

The α knockout process has been intensively investigated with quasifree $(p, p'\alpha)$ reactions, which provide clear information about kinematics. Comprehensive experimental studies have been conducted for the coincident measurements of $(p, p'\alpha)$ reactions. At proton energies of around 50 MeV, the reactions on targets of $A \geqslant 12$ are dominated by the sequential process [11–13]: The incident proton interacts with the target nucleus and then leaves it, whereupon the α particle is emitted via the sequential decays of the excited nucleus. The typical feature of the direct knockout dynamics has been observed in experiments at 100 MeV [14] and higher [15–20]. At 156 MeV, α particles with energies of at most 40 MeV were observed [18] coincident with protons, and they showed evidence of the direct knockout process. At higher incident energy [17], more contributions from the inner shell have been confirmed.

The mechanisms of other types of cluster production reaction have also been investigated with observational evidence. A representative example is the inclusive (p, dx) reactions; see Ref. [21] and the references therein. Many experimental studies have been conducted to explore the deuteron production mechanism by systematically measuring the energy spectra of double-differential cross sections (DDXs). Large amounts of experimental observations suggest that direct pickup is

dominant for reactions at impinging energies of 50 MeV or less. However, first-order DWBA analyses fail to account for the continuum spectra. The knockout contribution appears at around 90 MeV, is comparable with that of direct pickup at around 120 MeV, and is dominant above 200 MeV. For the higher-energy reactions, indirect pickup appears in the low-energy portion of the spectrum and then contributes more with increasing incident energy.

In our recent study [21], we explained the continua of (p, dx) reactions by means of a theoretical model that was developed based on the intranuclear cascade (INC) model. This INC-based model involves pickup, knockout, and indirect pickup and was applied to inclusive (p, dx) reactions at incident energies of 40–400 MeV. Although the ordinary INC model is used for reactions at 200 MeV or higher, we have extended the model [22–24] to energies below 100 MeV by introducing physics that had been neglected in previous studies. The model calculations account well for DDX experimental data. Note that these three processes in the model show features consistent with those observed in the aforementioned experimental studies. Because the knockout process is modeled within a framework of two-body kinematics, less ambiguity is expected in identifying the knockout process in comparison with DWBA analyses.

Expanding this INC-based model is a promising approach for quantitatively understanding the roles of direct pickup and knockout of inclusive (p, α) reactions from 42 to 300 MeV on many target nuclei ranging from ^{12}C and ^{209}Bi. In the present work, we use the same method as that for (p, dx) reactions and extend it to $(p, \alpha x)$ reactions. Therefore, our α production model is suited to the present study. We have already included direct pickup [25], knockout [26], and indirect pickup [26]. Now we improve the descriptions of direct pickup and knockout to obtain a consistent exposition of $(p, \alpha x)$ reactions at incident energies below a few hundred megaelectronvolts. Within the conventional two-step model, the INC calculations are responsible for the fast process, and they are followed by an evaporation model (slow process) to calculate the entire energy range of DDX spectra. In this work, we use the generalized evaporation model (GEM) [27], whose role is essential in the low-energy range of the spectra; however, the GEM is beyond the scope of the present study.

II. MODEL

A. INC model extended to low energies

The most important features of our model are described in this section. The basic idea of the INC model is that proton-nucleus reactions are reduced to a series of *NN* collisions. The space-time evolution of the nuclear system is calculated on an event-by-event basis by means of the Monte Carlo method. The target nucleus is initially composed of nucleons whose positions and momenta are randomly chosen according to prescribed distributions. The momentum distribution is a zero-temperature Fermi gas in a square-well nuclear potential with a depth of $V_{np} = 45$ MeV. The nucleon density follows a Woods-Saxon distribution with a maximum nuclear radius of $R = r_0 + 5a_0$ with diffuseness $a_0 = 0.54$ fm and half-density radius $r_0 = (0.978 + 0.0206A^{1/3})A^{1/3}$ (fm) [28], where A is the atomic mass number. The Fermi energy is determined using the binding energy calculated with the Bethe-Weizsäcker mass formula. The impact parameter b of the projectile is chosen randomly within R. The energetic nucleons above the Fermi sea are propagated in space by means of classical mechanics. Intranuclear *NN* collisions are assumed to take place when two nucleons approach each other to within a distance less than $\sqrt{\sigma_{NN}/\pi}$, where σ_{NN} is the experimental *NN* collision cross section parameterized in [29]. An energetic nucleon at the nuclear surface can penetrate the potential barrier according to the transmission probability or can be reflected by the barrier. The reflected nucleon is assumed to be bound in an equilibrium state.

In the case of the $(p, p'x)$ reaction, the DDX is expressed by

$$\frac{d^2\sigma}{dE\,d\Omega}(\theta, \varepsilon) = \frac{\pi R^2}{2\pi\,\Delta E\,\Delta\cos\theta} P^p(\theta, \varepsilon), \tag{1}$$

where ΔE and $\Delta\cos\theta$ are the bin widths of the outgoing energy ε and the laboratory angle θ, respectively. The proton emission probability P^p in the present INC model [22–24] includes the physics essential for medium-energy reactions. In only nucleon degrees of freedom, the symbolic expression for P^p is given as

$$P^p(\theta, \varepsilon) = P^p_{\rm def}(1 + P_{CE})(G + GP_{NN}G + GP_{NN}GP_{NN}G + \cdots)P^p_{\rm tr}P^p_{\rm def}|_{\theta,\varepsilon}, \tag{2}$$

where the time order of the process is from left to right, and G is the space development operator for particles inside the target nucleus. Because of the square-well nuclear potential, particles move along a straight line inside the nucleus and are deflected when they cross the boundary of the nucleus. The proton deflection function $p^p_{\rm def}$ provides a deflection angle at the nuclear surface for both the entrance and the exit channels, which has been shown to reproduce the angular distribution of proton-nucleus elastic scattering. P_{CE} is the probability of energy transfer by collective excitations. P_{NN} is the in-medium *NN* collision probability to provide the energy and direction of the scattered nucleons, which are calculated as described above with the Pauli blocking operator:

$$\hat{Q}|ij\rangle = [1 - \Theta(E_i - E_F)][1 - \Theta(E_j - E_F)]|ij\rangle, \tag{3}$$

where E_i is the energy of nucleon i after the collision and E_F is the Fermi energy. Θ denotes the unit step function. $P_{\rm tr}$ is the barrier transmission probability for the escaping proton. The functions for proton emission are curtailed.

B. α production process

The α particle production process is attributable to direct pickup, knockout, and indirect processes. We assume that direct pickup and knockout take place in the initial-state interaction and that the indirect process takes place in the final-state interaction. Other interactions causing α-particle integration or disintegration are not considered. Therefore, the α emission probability is written as

$$P^\alpha = P^{\alpha,i} + P^{\alpha,f}, \tag{4}$$

where $P^{\alpha,i}$ and $P^{\alpha,f}$ are the α emission probabilities due to the initial- and final-state interactions, respectively.

The α emission probability due to the initial-state interaction in proton-induced reactions is written as

$$P^{\alpha,i}(\theta,\varepsilon) = P^{p}_{\rm def}(P_{dp} + \hat{Q}_{p+\alpha}P_{\rm ko})(G + GP_{\alpha N}G + GP_{\alpha N}GP_{\alpha N}G + \cdots)P^{\alpha}_{\rm tr}P^{\alpha}_{\rm def}\big|_{\theta,\varepsilon}, \quad (5)$$

where P_{dp} and $P_{\rm ko}$ are the probabilities for direct pickup and knockout, respectively. The probabilities are determined to fit the experimental data, and their details are explained in the following sections. These two processes are assumed to take place via the initial-state interaction, namely, the first interaction between the projectile and the target. $\hat{Q}_{p+\alpha}$ is the Pauli blocking operator for the in-medium $p+\alpha$; collision, where the particles i and j in Eq. (3) are respectively the incident proton and one of the four nucleons in the α particle, which have energy equal to one-fourth that of the α particle. Note that in this work the α particle is treated as a four-nucleon system inside the nucleus rather than as an elementary particle. This treatment is essential for reproducing the prominent quasifree bump observed in the 400-MeV region of (p, dx) spectra [26]. $P_{\alpha N}$ is the α-nucleon collision during α transport inside the nucleus, which is calculated under the assumption that the in-medium nucleon-α collision occurs via interaction between a nucleon and one of the nucleons of the α particle. Breakup of the α particle is disregarded. For α transport, G works on the center of mass of the α particle. The constituent nucleons move while maintaining their positions relative to the center of mass, but every particle potentially has its own momentum. $P^{\alpha}_{\rm tr}$ is the α transmission probability from inside to outside the nucleus, which is given by the unit step function at the Coulomb potential at a distance of $r_0 + 1.5$ fm from the center of the target nucleus. $P^{\alpha}_{\rm def}$ is the α deflection [30] at the nuclear surface when the α particle leaves the nucleus:

$$P^{\alpha}_{\rm def} = \exp\left[-0.001(1.2\varepsilon - 10\ln A + 40)\theta\right]. \quad (6)$$

The Q value of the reaction and the recoil of the residual nucleus are taken into consideration as a final-state interaction after the cascade process is terminated.

C. Direct pickup of triton

The triton pickup process for (p,α) reactions is described in a similar way to that for the (p, d) reaction [21]. We assume that the residual nucleus is in a (ν^{-2}, π^{-1}) state. The energy E_α of the α particle just after pickup is given by

$$E_\alpha = E_{\rm p} - U, \quad (7)$$

where $E_{\rm p}$ is the energy of the incident proton. The excitation energy U of the nucleus is given by

$$U = E_F - E_t, \quad (8)$$

where E_F and E_t are the Fermi energy and the single-particle energy of transferred triton, respectively. By assuming that the maximum excitation energy $U^{\rm max}$ is due to the deepest-hole state, we define the probability P_{dp} as

$$P_{dp} = N\int_0^{U^{\rm max}} [W_{\rm low}(U) + kW_{\rm high}(U)]dU. \quad (9)$$

The weighting factor k, which is introduced to choose low- or high-excitation states, and the normalization factor N are determined by fitting to the energy spectra according to the incident energy and the target nucleus. These two parameters are essential for reproducing the DDXs.

The population of low-lying states is calculated by the Breit-Wigner function:

$$W_{\rm low}(U) = \frac{\Gamma^2}{(U - E_{\rm peak})^2 + \Gamma^2}, \quad (10)$$

which is known to describe the high susceptibility of strong transitions to low-excitation states. We choose the peak energy $E_{\rm peak}$ and the width Γ to be 0 and 2 MeV, respectively, in order to fit the spectral shapes near the ground state for a large amount of experimental DDX data. Although setting these parameters at the fixed values independently of the target and incident energy is a crude approximation, it is reasonable for considering DDXs, in which details of the shell structure are smeared out. The excitation energy of highly excited states is given by

$$W_{\rm high}(U) = s(U)\rho(U), \quad (11)$$

where $\rho(U)$ is the state density given by the Williams' formula [31] and $s(U)$ is the damping factor of the transition strength to the highly excited state. These two functions are expressed by

$$\rho(U) = \frac{[U - 0.25(p^2 + h^2 + p - 3h)]^{p+h-1}}{p!h!(p+h-1)!} \quad (12)$$

for the excited states of p particles and h holes, and

$$s(U) = \begin{cases} 1, & 0 < U < V_F, \\ \frac{U^{\rm max} - U}{U^{\rm max} - V_F}, & V_F \leqslant U < U^{\rm max}, \end{cases} \quad (13)$$

respectively. We calculated $\rho(U)$ with $p = 0$ and $h = 3$, and $s(U)$ with $U^{\rm max} = 3V_{np}$ and $V_F = 3E_F$. It is assumed that the momentum direction of the produced α particle is given by the added vector of the incident proton and the transferred nucleons.

D. Knockout of α particle

The knockout calculation is in principle the same as that in Refs. [21,26], which assumes the existence of an α particle in the target nucleus. A preformed α particle is prepared at the nuclear surface before the proton-α collision. This α particle is composed of two protons and two neutrons located closest to the proton arrival position. We then reassign their locations and momenta: the location of one is to be the arrival position, the location of the others are determined randomly within a sphere of α-particle radius (1.8 fm), and their momentum magnitudes are determined so as to correspond to the on-shell single-particle energy given by Eq. (11) with parameters of $p = 0$ and $h = 4$ for $\rho(U)$ in Eq. (12), and $U^{\rm max} = 4V_{np}$ and

TABLE I. Experimental data (target and incident energy) used for analysis.

Target	Incident energy (MeV)
^{12}C	42, 62, 68
^{27}Al	28.8, 42, 61.7, 68, 90, 120, 160, 200
^{58}Ni	42, 68, 90
^{59}Co	120, 160, 200
^{89}Y	61.5
^{90}Zr	42, 68, 90
^{93}Nb	100
^{109}Ag	300
^{197}Au	61.7, 68, 120, 160, 200
^{209}Bi	38.7, 42, 61.7, 90

$V_F = 4E_F$ for $s(U)$ in Eq. (13). The direction of each momentum is kept unchanged. Because the α particle is treated as a group of four nucleons, their binding energies are not considered here. Note that the reassignment of locations and momenta is performed when knockout is chosen by the Monte Carlo method, the purpose of which is to reasonably treat intranuclear α-particle transport. Because α-particle knockout occurs with probability of less than 1% out of all proton-nucleus reactions, the reassignment does not affect the other reaction channels. It has been confirmed that other reactions including the production of clusters (d, t, ^{3}He, and α) can be calculated with good accuracy by the same simulation.

The proton-α collision is assumed as the collision between the incoming proton and the α constituent nucleon nearest to the incoming proton. The energy of the virtually scattered α particle is given by the sum of the energies of the four nucleons. For the Pauli blocking judgment according to Eq. (3), $\hat{Q}_{p+\alpha}$ is applied to one-fourth the energy of the α particle as well as the energy of the proton (the collision partner). If the collision is blocked, all the particles involved in this virtual scattering are returned to their original state. The direction of the α-particle momentum is calculated as the vector sum of the four nucleons.

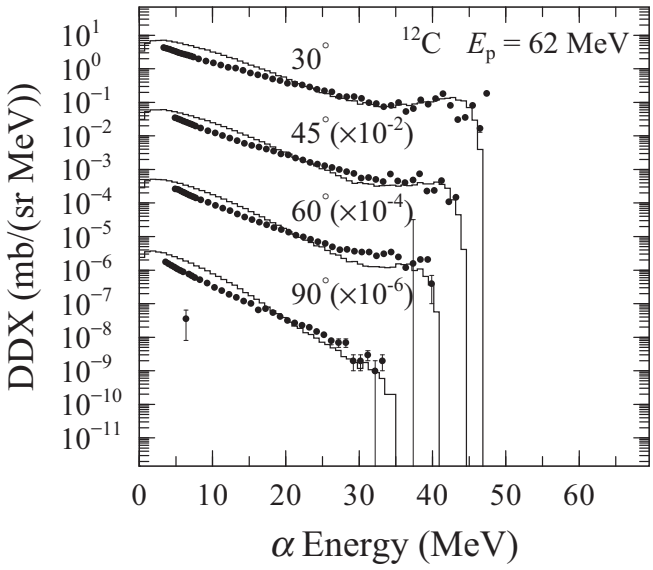

FIG. 1. Spectra of the 62-MeV ^{12}C$(p, \alpha x)$ reaction at 30°–90°. Lines and dots show results of present model and experiment, respectively. The multiplicative factors indicated in the figure were used to avoid overlap.

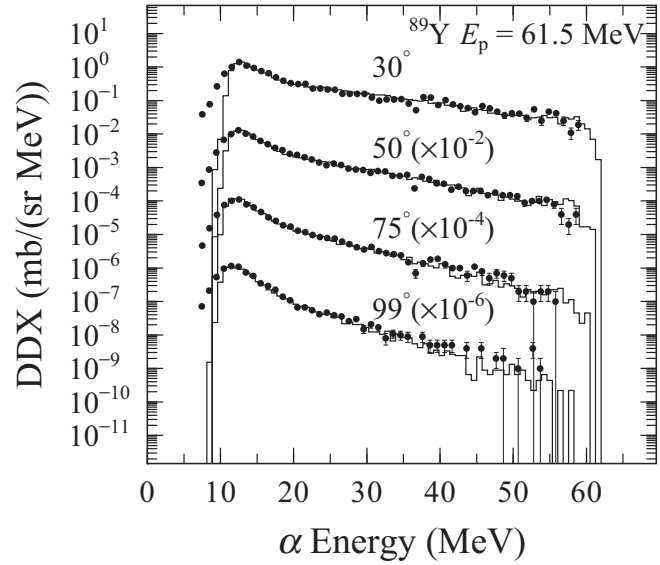

FIG. 2. Same as Fig. 1 but for the 61.5 MeV ^{89}Y$(p, \alpha x)$ reaction at 30°–99°.

E. Indirect pickup

Indirect pickup is considered to be a final-state interaction and is known to be responsible for the low-energy part of the spectra of proton-nucleus reactions above a few hundred megaelectronvolts. This process is included in the present

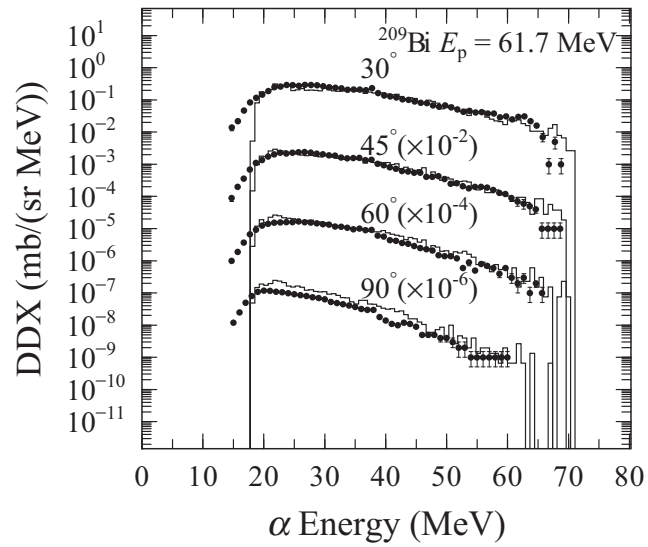

FIG. 3. Same as Fig. 1 but for the 61.7 MeV ^{209}Bi$(p, \alpha x)$ reaction at 30°–90°.

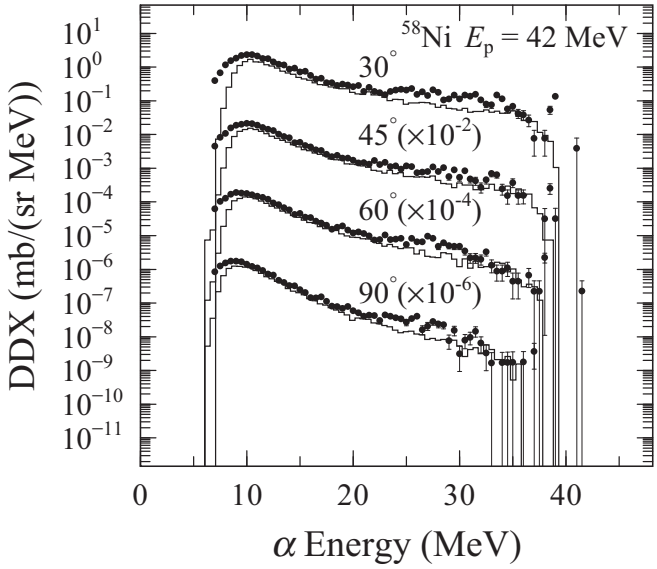

FIG. 4. Same as Fig. 1 but for the 42-MeV ^{58}Ni$(p, \alpha x)$ reaction at 30°–90°.

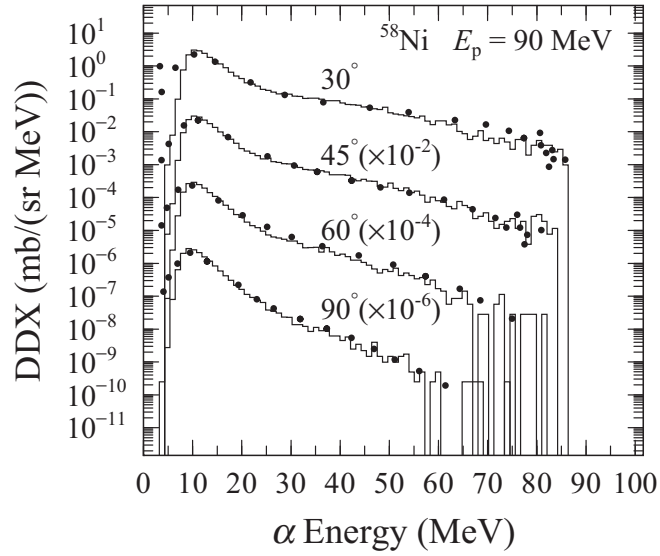

FIG. 6. Same as Fig. 1 but for the 90-MeV ^{58}Ni$(p, \alpha x)$ reaction at 30°–90°.

model, and its implementation is described in Ref. [26]. The α emission probability due to the final-state interaction in proton bombardment is written as

$$P^{\alpha,f}(\theta,\varepsilon) = P^{p}_{\rm def}(GP_{NN}G + GP_{NN}GP_{NN}G + \cdots) \times P^{N}_{\rm tr}P^{\alpha}_{id}P^{\alpha}_{\rm tr}P^{\alpha}_{\rm def}\big|_{\theta,\varepsilon} + P^{p}_{\rm def}P_{CE}(G + GP_{NN}G + GP_{NN}GP_{NN}G + \cdots) \times P^{N}_{\rm tr}P^{\alpha}_{id}P^{\alpha}_{\rm tr}P^{\alpha}_{\rm def}\big|_{\theta,\varepsilon}, \quad (14)$$

where $P^{N}_{\rm tr}$ is the nucleon transmission probability and P^{α}_{id} is the α formation probability due to indirect pickup. According to Eq. (14), a nucleon that has sufficient kinetic energy to leave the nucleus after any interactions is able to pick up other nucleons at the exit. The calculation algorithm of this process is similar to, but simpler than, that of the coalescence method employed by molecular-dynamics models [32,33] and other INC models [34,35]. The basic assumption is that a cascade nucleon i escaping the target nucleus can pick up three other nucleons j having the proper isospins, if each of them fulfills the phase space condition

$$r_{ij}p_{ij} \leqslant \lambda, \quad (15)$$

where r_{ij} and p_{ij} are the relative position and momentum, respectively, of particles i and j, and λ is the clustering parameter, which is determined to be 3500 fm MeV/c. The

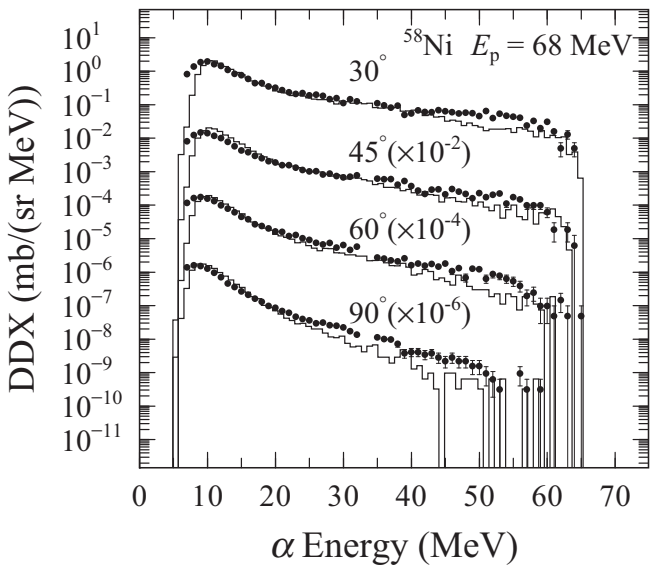

FIG. 5. Same as Fig. 1 but for the 68-MeV ^{58}Ni$(p, \alpha x)$ reaction at 30°–90°.

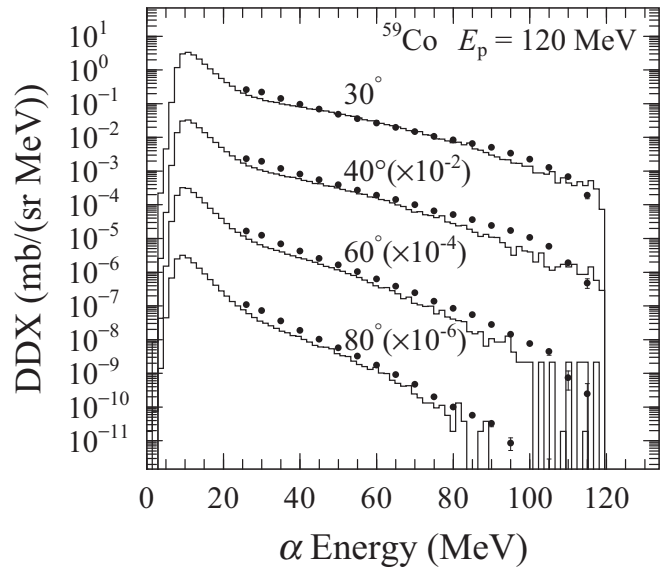

FIG. 7. Same as Fig. 1 but for the 120-MeV ^{59}Co$(p, \alpha x)$ reaction at 30°–80°.

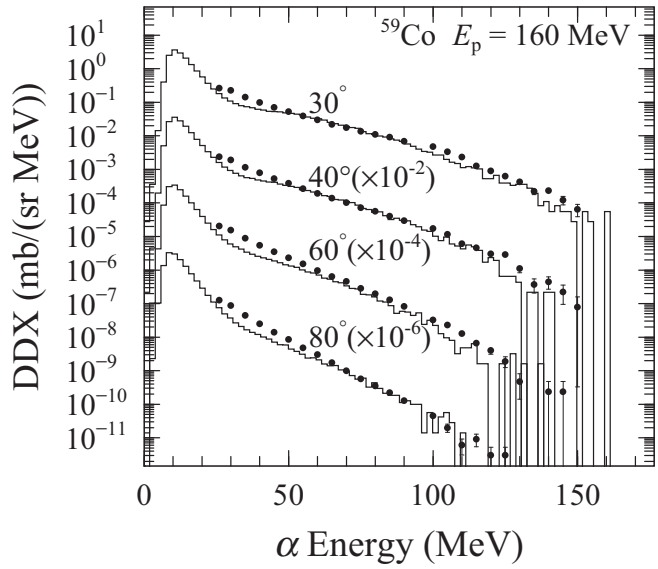

FIG. 8. Same as Fig. 1 but for the 160-MeV ^{59}Co$(p, \alpha x)$ reaction at 30°–80°

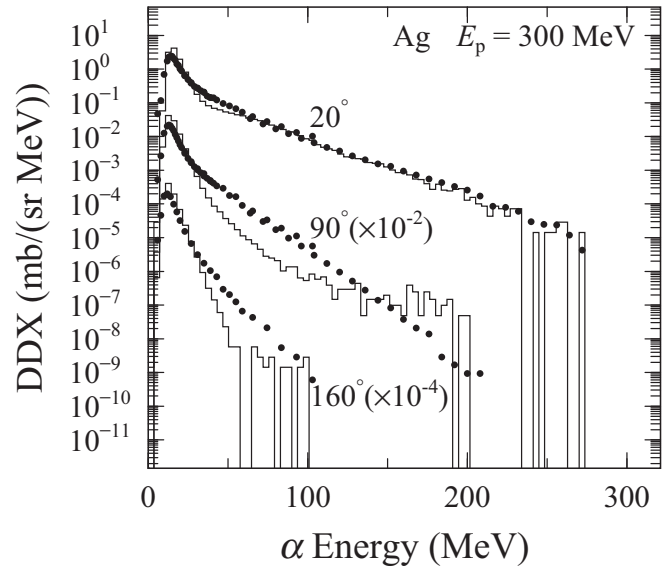

FIG. 10. Same as Fig. 1 but for the 300-MeV ^{nat}Ag$(p, \alpha x)$ reaction at 20–160°.

momentum of the α particle is given by the vector sum of the constituent nucleons. The energy is calculated from the momentum. If the energy is high enough to penetrate the barrier, indirect pickup occurs and the α particle is ejected. Otherwise, the leading nucleon i is emitted as a free nucleon, and nucleons in the α particle are set in their states before the clustering process.

III. RESULTS AND DISCUSSION

The calculated DDX spectra for $(p, \alpha x)$ reactions can be compared with various experimental data covering a wide range of incident energies and a wide range of the mass of the target nucleus. In the present work, we used the data listed in Table I. The experimental data are cited from Ref. [36] for experiments [4,37–41]. The resultant spectra for 62-MeV $(p, \alpha x)$ reactions on ^{12}C, ^{89}Y, and ^{209}Bi are displayed as solid lines in Figs. 1–3, respectively. The experimental data are indicated by dots. The measured laboratory angles and some factors depending on the angles are multiplied to avoid overlap are indicated in the figures. Similar comparisons for the different incident energies are displayed in Figs. 4–9 from 42 to 200 MeV. The results for incident energies of 42, 68, and 90 MeV on the ^{58}Ni target are shown in Figs. 4–6, respectively. The spectra at 120, 160, and 200 MeV on the

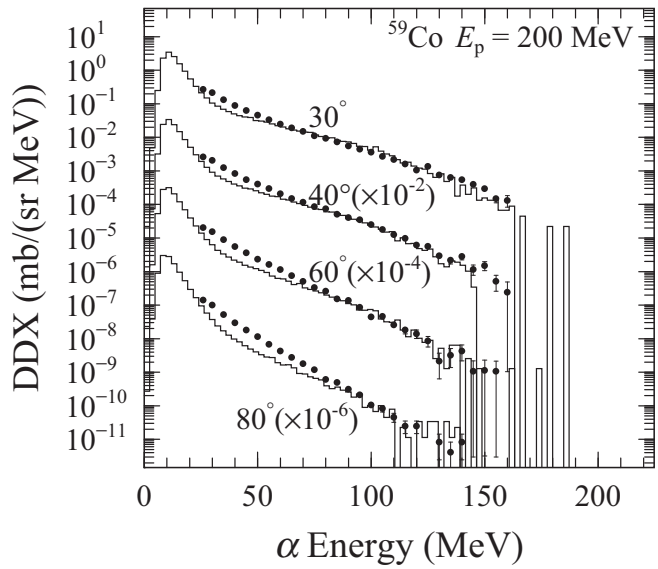

FIG. 9. Same as Fig. 1 but for the 200-MeV ^{59}Co$(p, \alpha x)$ reaction at 30°–80°.

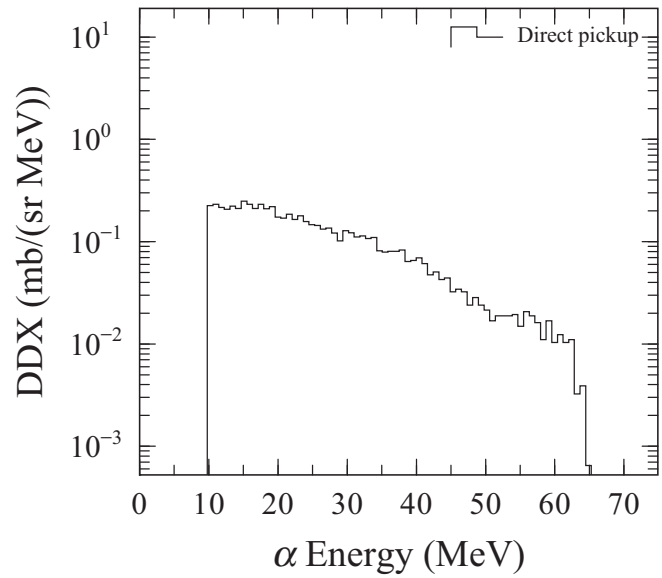

FIG. 11. Direct pickup component (solid line) for the 68-MeV ^{58}Ni$(p, \alpha x)$ reaction at 30° and evaporation component (broken line).

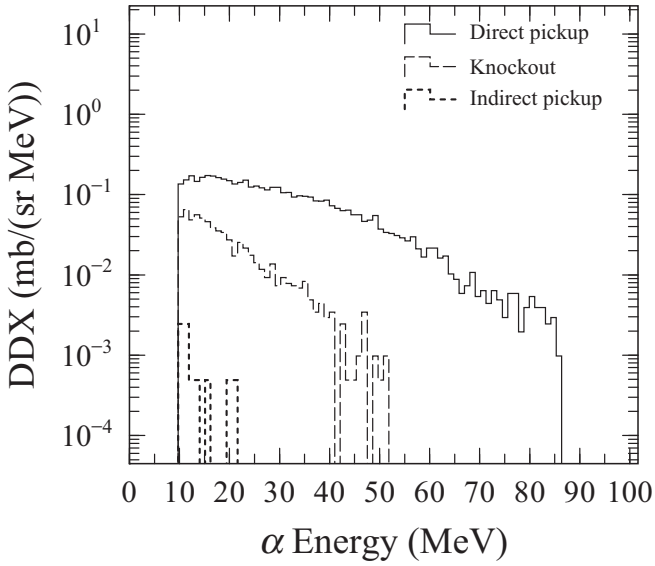

FIG. 12. Components of direct pickup (solid line), knockout (broken line), and indirect pickup (dotted line) for the 90-MeV ^{58}Ni$(p, \alpha x)$ reaction at 30°.

^{59}Co target are shown in Figs. 7–9, respectively. Figure 10 shows a comparison of the 300-MeV ^{nat}Ag$(p, \alpha x)$ reaction. The calculation results reproduce the experimental data fairly well at all angles and over the entire energy range, although slight inconsistencies are observed in the highest energy region and the evaporation region. At the highest energies in the forward-angle spectra, the scatter in the experimental data is due to discrete-level structures.

The contributions of direct pickup, knockout, and indirect pickup are shown by the solid, broken, and dotted lines, respectively, in Figs. 11–15 for incident energies of 68, 90, 120, 160, and 200 MeV, respectively. Figures 11 and 12 show the results on the ^{58}Ni target, and Figs. 13–15 show the results on the ^{59}Co target. The evaporation yields are not displayed. At energies of 42 and 68 MeV, direct pickup occupies the entire range and knockout is negligible, therefore the 42-MeV result is omitted. As shown in Figs. 12 and 13, the yields of knockout and indirect pickup appear and increase with increasing energy from 90 to 120 MeV, but both are still negligible in comparison with direct pickup. Figure 14 shows that at 160 MeV, knockout contributes as much as direct pickup, and the knockout yield is larger than that of direct pickup in a narrow region just above the evaporation. At 200 MeV, Fig. 15 shows that the knockout extends its territory almost entirely. It is notable that the energy trend of knockout is

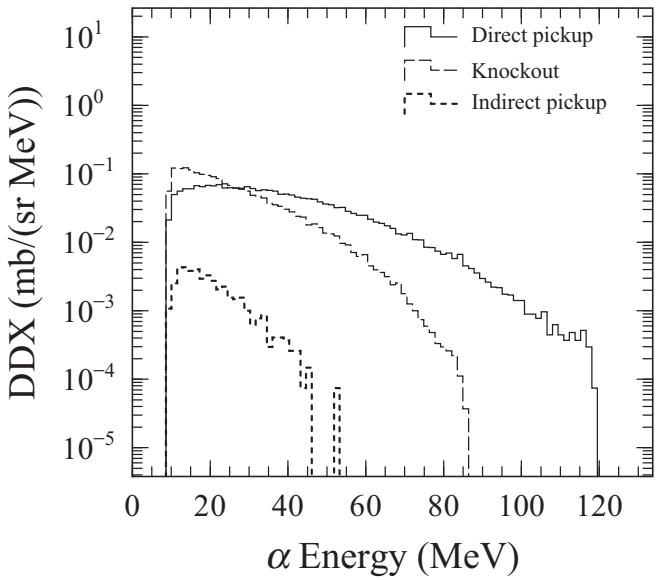

FIG. 13. Same as Fig. 12 but for the 120-MeV ^{59}Co$(p, \alpha x)$ reaction at 30°.

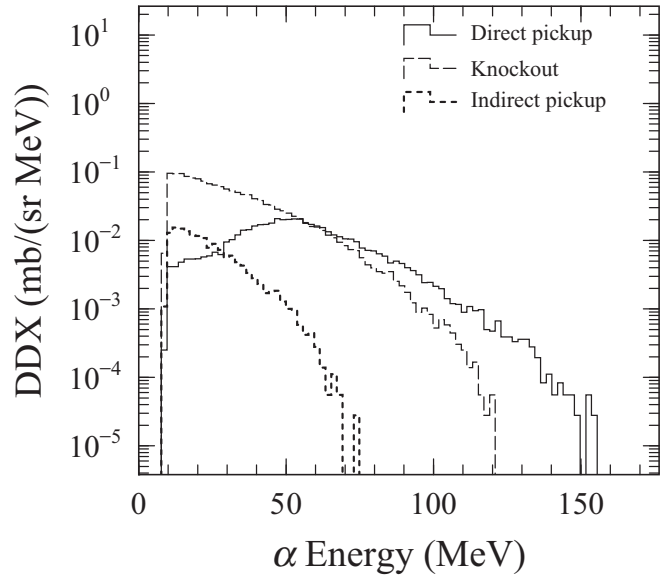

FIG. 14. Same as Fig. 12 but for 160 MeV.

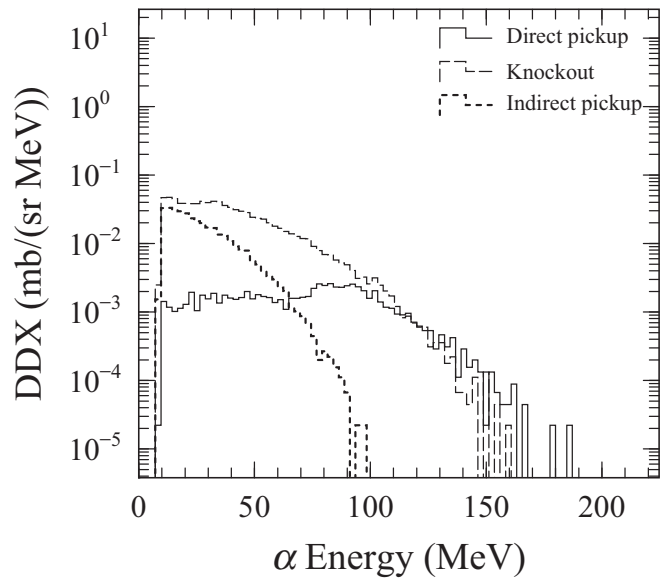

FIG. 15. Same as Fig. 12 but for 200 MeV.

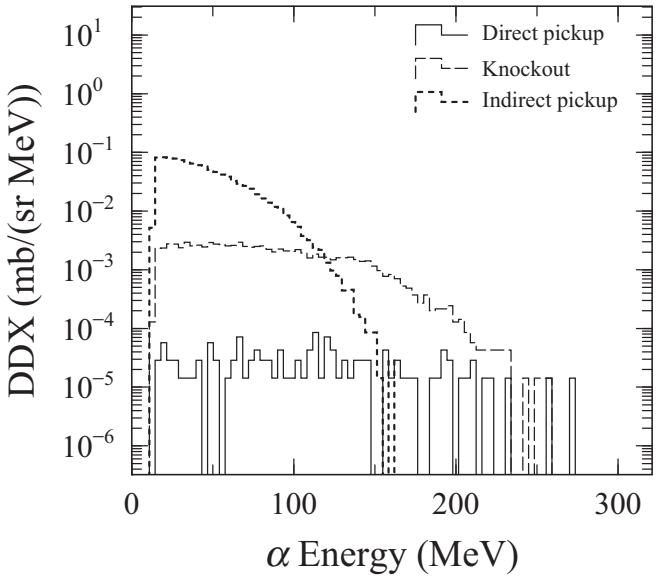

FIG. 16. Same as Fig. 12 but for 300-MeV Ag($p, \alpha x$) reactions at 20°.

qualitatively consistent with the results of (p, $p'\alpha$) studies. Figure 16 shows the 300-MeV results for the Ag target, which indicate that the knockout yield increases at higher energy, where the knockout is dominant, but the DDX values are small; alternatively, the indirect pickup grows steeply and occupies the low-energy part of the α spectrum, in which most of the α yield is consumed.

The resultant cross sections of low and high excitations in direct pickup are plotted in Figs. 17(a) and 17(b), respectively, for the targets of ^{12}C (•), ^{16}O (+), ^{27}Al (○), ^{58}Ni (•), ^{59}Co (□), ^{89}Y (■), ^{90}Zr (△), ^{93}Nb (▲), ^{109}Ag (▽), ^{120}Sn (▼), ^{197}Au (×), and ^{209}Bi (◇). The cross sections for low excitations decrease with the incident energy from 40 to 300 MeV. All targets show similar energy dependence to each other. In the results for high excitation, the cross sections are almost constant regardless of energy below 100 MeV, whereas they decrease with energy above 100 MeV. Moreover, they tend to increase with the target mass. The cross sections for knockout are displayed in Fig. 18 for nine targets from ^{27}Al to ^{209}Bi; the symbols in this figure are the same as those in Fig. 17. The cross sections decrease with the energy and tend to increase with the target mass. Both the pickup and knockout cross sections decrease with increasing energy, but the pickup cross sections decrease much faster than the knockout cross sections. With energy increasing from 50 to 300 MeV, the pickup cross sections decrease by three to four orders of magnitude, whereas the knockout cross sections decrease by only two orders of magnitude.

In this work, the ($p, \alpha x$) reaction was modeled with four processes: (a) direct pickup leading to low excitation, (b) direct pickup leading to high excitation, (c) knockout, and (d) indirect pickup. To describe these processes, we introduced six parameters that need adjustment to reproduce the experimental data. Four of these parameters, N, k, $P_{\rm ko}$, and λ, determine the magnitude of the DDXs. N and k are parameters in Eq. (9) for processes (a) and (b). $P_{\rm ko}$ and λ are parameters

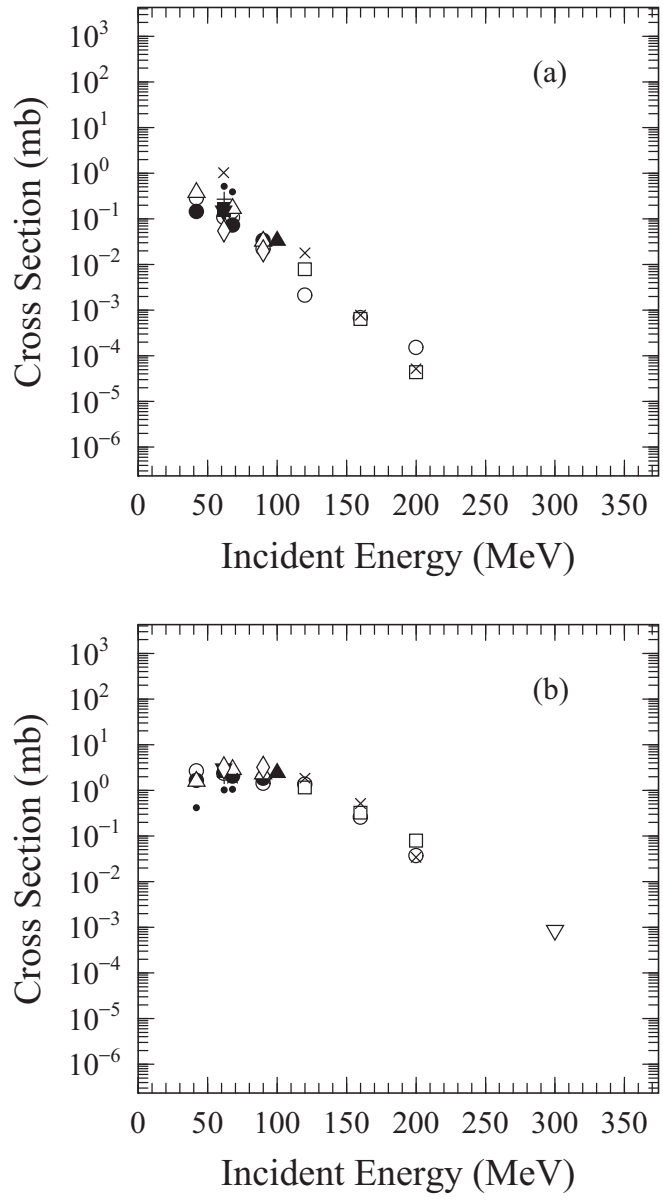

FIG. 17. (a) Cross sections of direct pickup leading to low excitations for various targets and incident energies. Symbols are defined in the text. (b) Cross sections of direct pickup leading to high excitations. Symbols are defined in the text.

for (c) and (d), respectively. The contributions of (a)–(c) are significant, meaning that N, k, and $P_{\rm ko}$ play essential roles. In contrast, the contribution of process (d) is unclear, because it is important at higher incident energies. In addition to these four parameters, we introduced two parameters $E_{\rm peak}$ and Γ in Eq. (10) for process (a), the cross sections of which are much smaller than those of processes (b) and (c). These parameters determine the spectral shape in a narrow region near the ground state, and thus their importance is not very high.

IV. CONCLUSION

We investigated the α-particle production mechanism by proton bombardment below 300 MeV. The processes of direct

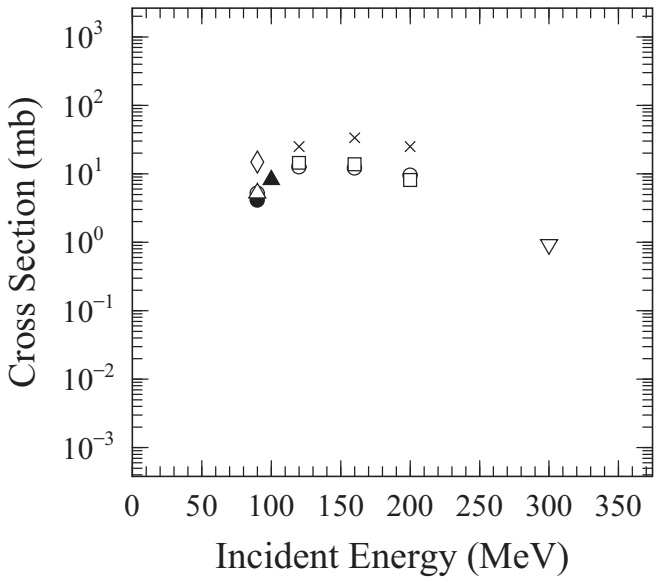

FIG. 18. Cross sections of knockout leading to low excitations in various targets and incident energies. Symbols are defined in the text.

pickup and knockout were modeled and incorporated into the INC model. The calculated DDX spectra agree well with the experimental DDXs over the entire ranges of emission energy and laboratory angle. The model reveals the contributions of pickup and knockout in terms of incident-energy dependence. Direct pickup accounts for the low-excitation-energy domain of the spectra. Knockout becomes increasingly important with incident proton energy. Its contribution is negligible below 120 MeV, dominates the narrow region of the spectrum at 160 MeV, and at 200 MeV is responsible for almost the entire range of the energy spectrum above the evaporation region. At 300 MeV, knockout occupies the higher energy part of the spectrum, where DDX values are small. Alternatively, indirect pickup is responsible for the large DDX region. Both direct pickup and knockout show incident-energy trends that are independent of the target over a mass range of 12 to 209. It is found that both direct pickup and knockout decrease with incident energy, but direct pickup decreases much faster than knockout.

[1] P. E. Hodgeson and E. Běták, Phys. Rep. **374**, 1 (2003).
[2] R. Bonetti, F. Crespi, and K.-I. Kubo, Nucl. Phys. A **499**, 381 (1989).
[3] E. Gadioli, E. Gadioli-Elba, P. Guazzoni, P. E. Hodgson, and L. Zetta, Z. Phys. A **318**, 147 (1984).
[4] S. S. Dimitrova, A. A. Cowley, E. V. Zemlyanaya, and K. V. Lukyanov, Phys. Rev. C **90**, 054604 (2014).
[5] H. Feshbach, A. Kerman, and S. Koonin, Ann. Phys. (NY) **125**, 429 (1980).
[6] S. S. Dimitrova, A. A. Cowley, J. J. van Zyl, E. V. Zemlyanaya, and K. V. Lukyanov, Phys. Rev. C **89**, 034616 (2014).
[7] A. A. Cowley, S. S. Dimitrova, E. V. Zemlyanaya, K. V. Lukyanov, and J. J. van Zyl, EPJ Web Conf. **107**, 08004 (2016).
[8] P. E. Hodgson, CERN Libraries, SCAN-9511244, 1995 (unpublished) https://cds.cern.ch/record/291865/files/SCAN-9511244.pdf.
[9] M. Nakano and Y. Uozumi, Phys. Rev. C **100**, 034619 (2019).
[10] M. Nakano, Y. Yamaguchi, and Y. Uozumi, Phys. Rev. C **101**, 044616 (2020).
[11] M. B. Epstein *et al.*, Phys. Rev. **178**, 1698 (1969).
[12] M. B. Epstein, J. R. Quinn, S. N. Bunker, J. W. Verba, and J. R. Richardson, Nucl. Phys. A **169**, 337 (1971).
[13] J. R. Quinn, M. B. Epstein, S. N. Bunker, J. W. Verba, and J. R. Richardson, Nucl. Phys. A **181**, 440 (1972).
[14] P. G. Roos, N. S. Chant, A. A. Cowley, D. A. Goldberg, H. D. Holmgren, and R. Woody, Phys. Rev. C **15**, 69 (1977).
[15] A. N. James and H. G. Pugh, Nucl. Phys. **42**, 441 (1963).
[16] C. Ruhla *et al.*, Phys. Lett. **6**, 282 (1963).
[17] B. Gottschalk and S. L. Kannenberg, Phys. Rev. C **2**, 24 (1970).
[18] D. Bachelier, M. Bernas, O. M. Bilaniuk, J. L. Boyard, J. C. Jourdain, and P. Radvanyi, Phys. Rev. C **7**, 165 (1973).
[19] D. Bachelier and J. L. Boyard, Nucl. Phys. A **268**, 488 (1976).
[20] G. Landaud, A. Devaux, P. Delpierre, J. Kahane, R. Sené, J. Yonnet, and R. Anne, Phys. Rev. C **18**, 1776 (1978).
[21] Y. Uozumi, Y. Yamaguchi, G. Watanabe, Y. Fukuda, R. Imamura, M. J. Kobra, and M. Nakano, Phys. Rev. C **97**, 034630 (2018).
[22] Y. Uozumi, T. Yamada, S. Nogamine, and M. Nakano, Phys. Rev. C **86**, 034610, (2012).
[23] Y. Uozumi, T. Yamada, and M. Nakano, J. Nucl. Sci. Technol. **52**, 264 (2015).
[24] Y. Yamaguchi, Y. Uozumi, and M. Nakano, Phys. Rev. C **100**, 034617 (2019).
[25] Y. Uozumi, T. Mori, A. Sonoda, and M. Nakano, EPJ Web Conf. **122**, 04001 (2016).
[26] Y. Uozumi, Y. Sawada, A. Mzhavia, S. Nogamine, H. Iwamoto, T. Kin, S. Hohara, G. Wakabayashi, and M. Nakano, Phys. Rev. C **84**, 064617 (2011).
[27] S. Furihata, Nucl. Instrum. Methods Phys. Res. B **171**, 251 (2000).
[28] J. W. Negele, Phys. Rev. C **1**, 1260 (1970).
[29] J. Cugnon, D. L'Hôte, and J. Vandermeulen, Nucl. Instrum. Meth. Phys. Res. B **111**, 215 (1996).
[30] M. J. Kobra, G. Watanabe, Y. Yamaguchi, Y. Uozumi, and M. Nakano, J. Nucl. Sci. Technol. **55**, 209 (2017).
[31] F. C. Williams, Nucl. Phys. A **166**, 231 (1971).
[32] J. L. Nagle, B. S. Kumar, D. Kusnezov, H. Sorge, and R. Mattiello, Phys. Rev. C **53**, 367 (1996).
[33] R. Mattiello, H. Sorge, H. Stöcker, and W. Greiner, Phys. Rev. C **55**, 1443 (1997).
[34] A. Letourneau, A. Bohm, J. Galin, B. Lott, A. Peghaire *et al.*, Nucl. Phys. A **712**, 133 (2002).
[35] A. Boudard, J. Cugnon, S. Leray, and C. Volant, Nucl. Phys. A **740**, 195 (2004).
[36] EXFOR/CSISRS Experimental Nuclear Reaction Data, http://www.nndc.bnl.gov/exfor/exfor00.htm.

[37] M. Harada *et al.*, J. Nucl. Sci. Technol. **39**, 393 (2002).
[38] F. E. Bertrand and R. W. Peelle, Phys. Rev. C **8**, 1045 (1973).
[39] J. R. Wu, C. C. Chang, and H. D. Holmgren, Phys. Rev. C **19**, 698 (1979).
[40] A. A. Cowley, G. J. Arendse, J. W. Koen, W. A. Richter, J. A. Stander, G. F. Steyn, P. Demetriou, P. E. Hodgson, and Y. Watanabe, Phys. Rev. C **54**, 778 (1996).
[41] R. E. L. Green, R. G. Korteling, J. M. D'Auria, K. P. Jackson, and R. L. Helmer, Phys. Rev. C **35**, 1341 (1987).